Observed anomalous atmospheric patterns in summers of unusual Arctic sea ice melt

AGU PUBLICATIONS

JGR

Journal of Geophysical Research: Atmospheres

RESEARCH ARTICLE

10.1002/2014JD022608

Key Points:
- Distinct atmospheric patterns in summers of anomalous Arctic sea ice melt
- Storms track more zonal in midlatitudes than into the Arctic
- A positive cloud feedback characterize the Arctic

Correspondence to:
E. M. Knudsen,
erlend.knudsen@gfi.uib.no

Citation:
Knudsen, E. M., Y. J. Orsolini, T. Furevik, and K. I. Hodges (2015), Observed anomalous atmospheric patterns in summers of unusual Arctic sea ice melt, *J. Geophys. Res. Atmos.*, *120*, 2595–2611, doi:10.1002/2014JD022608.

Received 24 SEP 2014
Accepted 20 FEB 2015
Accepted article online 26 FEB 2015
Published online 1 APR 2015

Observed anomalous atmospheric patterns in summers of unusual Arctic sea ice melt

Erlend M. Knudsen[1,2], Yvan J. Orsolini[2,3], Tore Furevik[1,2], and Kevin I. Hodges[4]

[1]Geophysical Institute, University of Bergen, Bergen, Norway, [2]Bjerknes Centre for Climate Research, Bergen, Norway, [3]Norwegian Institute for Air Research, Kjeller, Norway, [4]Department of Meteorology, University of Reading, Reading, UK

Abstract The Arctic sea ice retreat has accelerated over the last decade. The negative trend is largest in summer, but substantial interannual variability still remains. Here we explore observed atmospheric conditions and feedback mechanisms during summer months of anomalous sea ice melt in the Arctic. Compositing months of anomalous low and high sea ice melt over 1979–2013, we find distinct patterns in atmospheric circulation, precipitation, radiation, and temperature. Compared to summer months of anomalous low sea ice melt, high melt months are characterized by anomalous high sea level pressure in the Arctic (up to 7 hPa), with a corresponding tendency of storms to track on a more zonal path. As a result, the Arctic receives less precipitation overall and 39% less snowfall. This lowers the albedo of the region and reduces the negative feedback the snowfall provides for the sea ice. With an anticyclonic tendency, 12 W/m^2 more incoming shortwave radiation reaches the surface in the start of the season. The melting sea ice in turn promotes cloud development in the marginal ice zones and enhances downwelling longwave radiation at the surface toward the end of the season. A positive cloud feedback emerges. In midlatitudes, the more zonally tracking cyclones give stormier, cloudier, wetter, and cooler summers in most of northern Europe and around the Sea of Okhotsk. Farther south, the region from the Mediterranean Sea to East Asia experiences significant surface warming (up to 2.4°C), possibly linked to changes in the jet stream.

1. Introduction

With northern high-latitude temperatures rising nearly twice as fast as the global average (referred to as the Arctic amplification; AA) [*Serreze and Francis*, 2006], the Arctic is undergoing rapid changes [*Bekryaev et al.*, 2010; *Screen and Simmonds*, 2010]. Most evident is the reduction in summer sea ice [*Walsh*, 2014], which some climate models project to disappear within two to three decades [*Stroeve et al.*, 2012; *Wang and Overland*, 2012].

While external forcings like global warming contribute to sea ice loss, changes in Arctic sea ice also feed back onto the other components of the climate system [*Cohen et al.*, 2014, and references therein]. These include alterations in albedo and exchanges of heat, momentum, and water vapor [*Vihma*, 2014]. The ice-albedo feedback causes the Arctic Ocean to trap more heat with declining sea ice cover, delaying the freezeup in fall [*Stroeve et al.*, 2014]. Sea ice also acts as a lid, separating the relative warm ocean from the cold atmosphere through most of the year. With reduced sea ice cover, heat fluxes into the atmosphere enhance and destabilize the air column [*Serreze and Barry*, 2009a].

Consequences of the sea ice decline are both local and remote. While local effects emerge as enhanced upward turbulent heat fluxes and outgoing longwave radiation, remote impacts are more complex [*Screen et al.*, 2013]. The latter are often mixed with responses to many other local or remote factors influencing climate in the specific region, such as tropical variability. It is thus hard to isolate the effects of diminishing Arctic sea ice cover on midlatitude climate [*Screen and Simmonds*, 2013; *Cohen et al.*, 2014].

The observed and projected changes in the Arctic climate system vary over the season. While trends are negative for all months, the largest changes in Arctic sea ice extent have taken place in late summer to early fall [*Deser and Teng*, 2008a]. This is also the most synoptically active period of the year over the Arctic Ocean, leading to a distinct summertime Arctic Ocean Cyclone Maximum (AOCM) [*Serreze and Barrett*, 2008; *Orsolini and Sorteberg*, 2009].

Cyclones traveling into the Arctic strongly interact with the Arctic sea ice through their associated wind patterns and reciprocal effects on and of sea ice export and production [*Sorteberg and Kvingedal*, 2006]. They

have major impacts on precipitation, the radiation budget and cloudiness, in addition to poleward heat and moisture transport [*Bengtsson et al.*, 2006; *Sorteberg and Walsh*, 2008; *Budikova*, 2009]. Hence, summer cyclones are crucial for high-latitude climate in summer [*Mesquita et al.*, 2008].

Cyclone tracks in summer are climatologically more tightly confined and poleward located compared to storm tracks in winter [*Mesquita et al.*, 2008]. In summer, the heating contrast between the Eurasian continent and the Arctic Ocean helps to develop strong cyclone activity over northern Eurasia [*Wernli and Schwierz*, 2006].

Little attention has been paid to summertime Arctic sea ice and atmospheric circulation compared to wintertime [*Zhang et al.*, 2004]. Results from the few studies that have been undertaken on the impact of a diminishing sea ice cover have shown a relative anticyclonic pattern [*Ogi et al.*, 2010; *Screen et al.*, 2011], raised geopotential height, a weakening of the 500 hPa zonal winds and a general northward shift in the polar jet stream in the Arctic [*Tang et al.*, 2013]. In midlatitudes, *Screen* [2013] linked anomalously low sea ice to a southward displacement of the jet stream over Europe with wetter summers over northern Europe.

On the basis of these circulation changes, *Francis and Vavrus* [2012] and *Tang et al.* [2013] proposed a link between Arctic sea ice loss and extreme weather events at midlatitudes. However, these hypotheses have been the subject of considerable discussion [*Cohen et al.*, 2014; *Walsh*, 2014]. *Barnes* [2013] found no significant trend of the suggested connection and explained the inconsistency as possibly being due to the methodology. *Screen and Simmonds* [2013] also noted the strong dependence on conceptualization, while *Coumou et al.* [2014] used theoretical and observational arguments for increased quasi-resonant frequency of wave number 7 and 8 patterns.

In this study, we perform a composite analysis to isolate distinct atmospheric patterns during summer months of anomalous sea ice melt. Sea ice melt rather than sea ice extent is used as the former is a more direct measure of sea ice changes resulting from and leading to alterations in atmospheric patterns. Because we are investigating the simultaneous covariance between the sea ice and the atmospheric fields, it is hard to determine causality. Nevertheless, we establish connections between sea ice and those patterns based on known, physical mechanisms.

The paper is organized as follows: section 2 describes the data sets used and method to isolate summer months of anomalous Arctic sea ice melts. Section 3 describes how atmospheric parameters differ in high versus low melt months, followed by a discussion putting the emerging patterns into context of earlier studies in section 4. The paper concludes with section 5, which summarizes the results, discusses the uncertainties of the study and puts the results into a broader perspective.

2. Data Sets and Methods

The main data sets used in this study are the National Snow and Ice Data Center (NSIDC) sea ice data and the European Re-Analysis Interim (ERA-Interim) atmospheric data. Monthly averages are used except for daily sea ice extents and 6-hourly wind data for storm track analysis. The time period used is the last 35 years (1979–2013), with the extended summer season May through August (MJJA) being the season of interest.

NSIDC provides both sea ice extent (SIE) and concentration (SIC) data [*Cavalieri et al.*, 1996]. Linear interpolation from neighboring days is used to replace missing days over two periods: from 1 January 1979 to 9 July 1987 and from 3 December 1987 to 13 January 1988 due to every other day satellite measurements and data gaps caused by satellite data transmission problems.

Monthly sea ice melt rate is defined as the difference of the SIE from the first to the last day of the month. This is positive for all the months in MJJA. Subtracting the averaged monthly melt rate and dividing by the standard deviation (STD) of the monthly melt rate, we calculate standardized monthly sea ice melt rates. Using a threshold of ± 1, we define months of anomalous high (HMR) and low (LMR) melt rates. They constitute 23 and 17 of the 140 MJJA months from 1979 to 2013, respectively (Figure 1).

Note that months with high (low) sea ice melts do not necessarily have to be in the years with low (high) sea ice cover. Although this is normally the case, as seen from the predominance of HMR months in latest year of

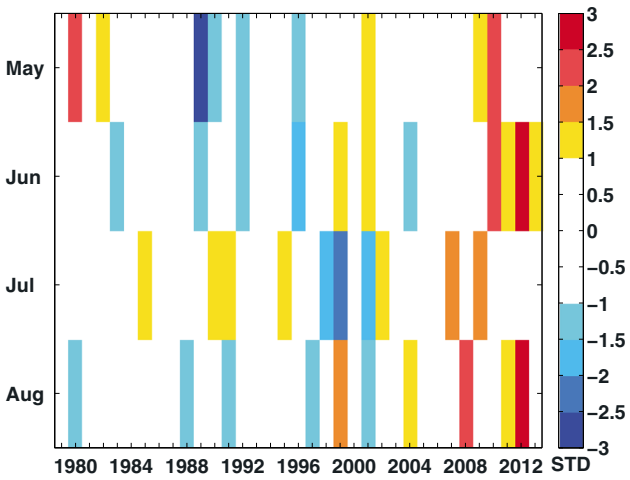

Figure 1. Standardized sea ice melt rate of months MJJA 1979–2013. Yellow to red colors indicate HMR months and cyan to blue colors LMR months, with color bar numbers representing standard deviations (STDs) from monthly averages.

the record, high (low) melt rate can also be explained by anomalously large (small) sea ice cover at the start of the month. This feature is depicted in Figure 2a. The largest positive anomaly occurs in the Pacific sector around the Bering Sea and the Sea of Okhotsk, where the ice edge is located around 1 May. Conversely, SIE and SIC at the end of the month is likely to be anomalously small in HMR months, as seen for August in Figure 2b. Again, most of the differences occur in the marginal ice zone, which for the end of August are all the marginal seas of the Arctic Ocean.

Consequently, a LMR month can be followed by a HMR month, and vice versa. This happened in 1999, when June and August were HMR months and July was a LMR month (Figure 1).

The data are not detrended, as indicated by the overrepresentation of HMR months in recent summers in Figure 1. There are two reasons for this (1) we want to perform an analysis of unmasked atmospheric signals in summers of anomalous Arctic sea ice melt and (2) the nonlinearity of the sea ice trend makes it difficult to remove trends without making spurious anomalies.

The parameters from ERA-Interim are mean sea level pressure (MSLP), components of zonal (u) and meridional (v) wind at 10 m, 850 hPa, and 300 hPa, 300 hPa geopotential height (Z), skin temperature (hereafter referred to as surface temperature; T_s), total precipitation, and snowfall. Additionally, the analysis includes incoming shortwave (SW) and longwave (LW) radiation at the surface.

Described in more detail by *Dee et al.* [2011], the ERA-Interim data set is a high-resolution reanalysis in space and time. In this study, a 0.50° × 0.50° grid is used for all fields, interpolated from the highest spatial

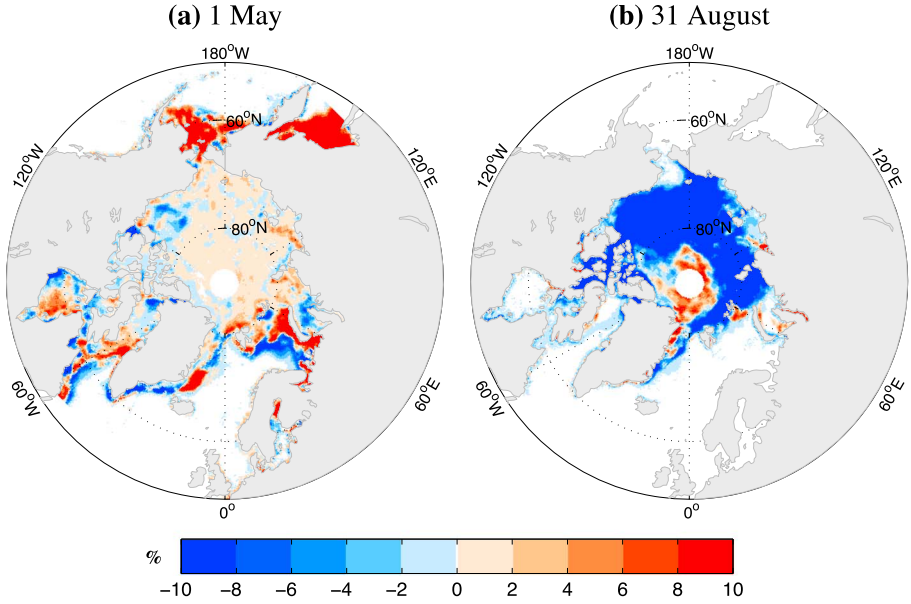

Figure 2. Sea ice concentration composite anomalies (a) for 1 May in 1979–2013 years with HMR in May and (b) for 31 August in 1979–2013 years with HMR in August.

resolution of 0.75° × 0.75° grid in the available ERA-Interim data. The data set is well suited for the northern regions [*Chung et al.*, 2013], especially for storm tracking [*Hodges et al.*, 2011; *Zappa et al.*, 2013].

The storm track analysis draws upon cyclone statistics derived using the TRACK algorithm described by *Hodges* [1994, 1995, 1999]. It uses 6-hourly relative vorticity (ζ) at 850 hPa to identify and track cyclones, here calculated from the *u* and *v* fields. Rather than MSLP, ζ is chosen for tracking since it does not depend on extrapolation to any large extent, is less influenced by the large-scale background pressure field, and focuses on the small-scale end of the synoptic range.

However, the ζ field at moderate to high resolution can be very noisy. Hence, the analysis is performed at a spectral resolution of T42 on a Gaussian grid. This allows the same spatial synoptic scales to be identified independent of the data set used. To focus on the synoptic variability, planetary scales with wave numbers below 5 and above 42 are removed. In addition, the cyclones must fulfill criteria regarding their displacement distance (minimum 1000 km) and lifetime (minimum 2 days). Only cyclones (not anticyclones) are considered.

Four Eulerian statistical fields are of interest: the track density (a measure of how many cyclones that pass through a region), the mean intensity (a measure of the strength of the cyclone), the genesis density (a measure of how many cyclones that form in a region), and the lysis density (a measure of how many cyclones that die out in a region). These are computed by the spherical kernel estimators described in *Hodges* [1996]. While the mean intensity unit corresponds to relative vorticity (10^{-5} s^{-1}), the density fields are given in units of number density per month per unit area where the unit area is equivalent to a 5° spherical cap ($\sim 10^6$ km^2). Although changes in the density fields also could result from more (less) tightly confined cyclones, they are more likely due to an increase (decrease) in the number of cyclones. Hence, in the following, we refer to changes in the density fields as more or fewer cyclones.

The HMR and LMR months are drawn noncoherently from a time series. According to *Neyman and Pearson* [1933], the Student's *t* test is the optimum for performing statistical significance test on this composite analysis. Accordingly, significance in most figures result from a two-sided *t* test on a 5% significance level. For the storm track characteristics, *p* values (the probability that a more extreme value is possible) are computed using a permutation Monte Carlo approach (sampling without replacement) [*Hodges*, 2008]. Correspondingly, grid points with $p < 0.05$ indicate significance in Figure 6.

3. Results

In this section, the atmospheric patterns in HMR and LMR months are shown for 20°N–90°N (40°N–90°N for precipitation). The maps show primarily composites of HMR minus LMR months to emphasize the patterns occurring for events of rapid sea ice retreat. Most panels show the average over all anomalous months, i.e., 23 and 17 months, respectively, with statistical significance based on these 40 months. Regions that are significant at the 5% level are marked with black and white dots.

3.1. Atmospheric Circulation

Higher sea ice melt corresponds to a significant anticyclonic tendency over the Arctic Ocean (up to 7 hPa higher in HMR compared to LMR; yellow to red colors in Figure 3a). The corresponding wind field (vectors in Figure 3a) is a good estimator of sea ice drift, which generally goes 30° to the right of the near-surface wind [*Nansen*, 1902].

The influence of wind on Arctic sea ice is largest in summer due to the little contact of the ice pack with the coast, thin ice, and large areas of open water at this time of year [*Thorndike and Colony*, 1982; *Ogi et al.*, 2010]. Consequently, the atmospheric circulation in HMR months favors a redistribution of sea ice from the heavy sea ice region north of Greenland and Ellesmere Island into the marginal seas, where it is more prone to melting (Figure 3a). Moreover, the remaining sea ice in the eastern Arctic Ocean is pushed toward the North Atlantic Ocean through the Barents Sea and the Fram Strait. However, the ice export through the Fram Strait in MJJA is less than 3% of the total sea ice melt (estimate based on *Smedsrud et al.* [2011]).

To relate the atmospheric pattern over the Arctic in Figure 3a to other patterns of variability in the region, we compared our standardized sea ice melt rate index with the standardized North Atlantic Oscillation (NAO) (National Oceanic and Atmospheric Administration (NOAA)/National Centers for Environmental Prediction (NCEP)/Climate Prediction Center (CPC), North Atlantic Oscillation (NAO), 2012, subset MJJA

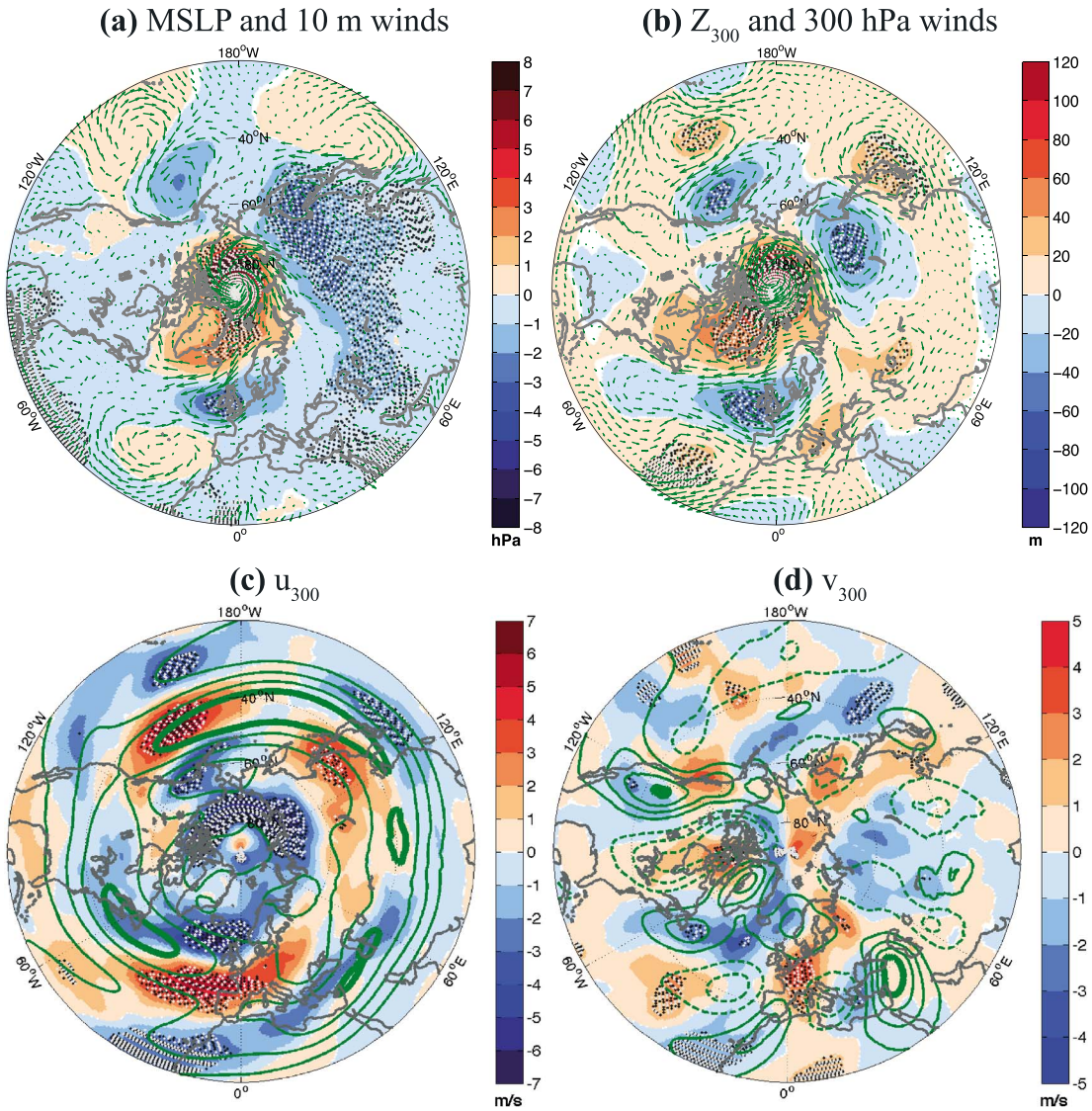

Figure 3. (a) Mean sea level pressure (MSLP; shading) and 10 m wind (vectors), (b) 300 hPa geopotential height (Z_{300}; shading) and wind (vectors), (c) zonal wind (u_{300}), and (d) meridional wind (v_{300}) composites for HMR minus LMR months for MJJA 1979–2013. Green contours in Figures 3c and 3d mark climatology over 1979–2013, where solid (dashed) lines indicate positive (negative) values. Contour intervals are 5 m/s in Figure 3c and 1.5 m/s in Figure 3d, with bold contours for visual clarity representing 20 m/s and 6 m/s, respectively. Alternating black and white dots mark regions of significant difference at a 95% confidence level.

1979–2013, available at http://www.cpc.ncep.noaa.gov/data/teledoc/nao.shtml), Arctic Oscillation (AO) (NOAA/NCEP/CPC, Arctic Oscillation (AO), 2005, subset MJJA 1979–2013, available at http://www.cpc.ncep.noaa.gov/products/precip/CWlink/daily_ao_index/ao.shtml), and Beaufort Sea High (BSH) (here defined as MSLP over 70°N–85°N, 160°E–100°W) over all MJJA months. Correlation analysis reveals that none of these patterns explain more than 10% of the variance in sea ice melt as defined here (explains 5%, 10%, and 10%, respectively). Hence, the sea ice melt rate index is largely independent of these climate patterns.

Outside the Arctic, HMR months are generally associated with lower MSLP (Figure 3a). More cyclonic tendencies over the Gulf of Alaska (−1 hPa; here defined 55°N–60°N, 137°W–163°W) and northwestern Europe (−2 hPa; here defined 47.5°N–61.5°N, 10°W–15°E), as well as a MSLP decrease over most of Eurasia (minimum of −3 hPa over the Sea of Okhotsk) all coincide with increased Arctic sea ice melting.

At 300 hPa, Figure 3b shows a significant positive Z anomaly over the Arctic in HMR compared to LMR months (up to 111 m). Correspondingly, the 300 hPa geopotential heights (Z_{300}) are down to 61 m lower over northwestern Europe and Asia and in the Gulf of Alaska. The resemblance to Figure 3a indicates

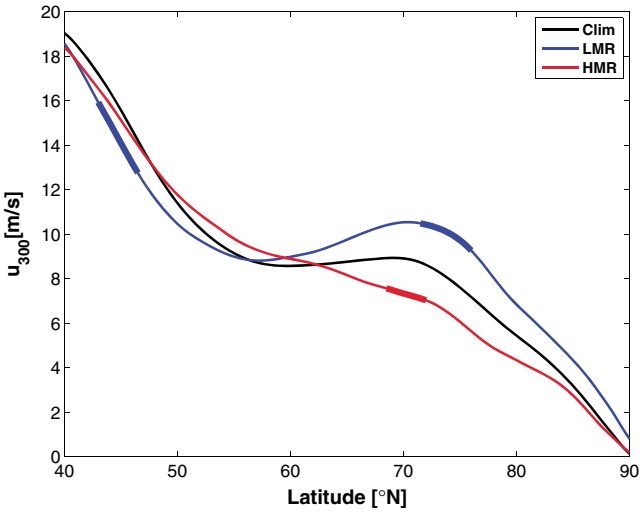

Figure 4. 300 hPa zonal wind composites of climatology (black), LMR (blue), and HMR (red) months zonally averaged over Eurasia (0–180°E) for MJJA 1979–2013. Thick curves indicate LMR and HMR months values significantly different to the climatology (Clim) at a 95% confidence level.

a barotropic pattern. This is also shown by a close similarity between Z_{300} (Figure 3b) and the 500 hPa geopotential height (Z_{500}) patterns (not shown).

In Figure 3c, the shadings present the composite difference of 300 hPa zonal winds for HMR minus LMR months, while the contours indicate the locations of the climatological jet streams. Compared to LMR months, there is a 31% decrease in zonal winds (u_{300}) over the Arctic (here defined circumpolar north of the Arctic Circle) in HMR months, in particular over the region where the AOCM normally is found. There is also a southward shift of the jet over the North Atlantic Ocean, with the jet following a more zonal path from the North Atlantic Ocean to the Far East.

The changes in the zonal winds across Eurasia are further detailed in Figure 4. It reveals that the distinct climatological subpolar jet across Eurasia vanishes in HMR months, while significantly strengthens in LMR months. Conversely, u_{300} is significantly weakened around 45°N in LMR months. The Asian jet core at about 40°N, however, remains unchanged in HMR compared to LMR months.

The climatological 300-hPa meridional winds (v_{300}) in Figure 3d (contours) show the location of the near-stationary wave trains. Two circumglobal wave trains are found at high- and midlatitudes, along the subpolar and subtropical jet streams. Across Eurasia, the wave trains have out-of-phase centers in the meridional direction, where the wave train along the Asian jet is also known as the Silk Road Pattern [*Enomoto et al.*, 2003].

In midlatitudes, the most significant change is a weakening of the wave trains over North America, the North Atlantic Ocean and Europe, as indicated by the bluish (reddish) color overlying solid (dashed) lines in Figure 3d. Over Europe, this weakening is accompanied by a southeastward shift, with a tendency of a more southerly meridional flow. Moreover, the changes coincide with a more zonal jet over the North Atlantic Ocean (Figure 3c) and its northward veering at the eastern branch of the relative cyclone centered over the British Isles (Figure 3b). Correspondingly, the relative trough and ridges in the North Pacific Ocean (Figure 3b) also have significant anomalies in zonal and meridional winds at 300 hPa (Figures 3c and 3d).

3.2. Storm Track Characteristics

Figure 5 shows the tracks of the strongest cyclones in HMR (Figure 5a) and LMR (Figure 5b) months. Common for the two panels is the density of cyclone tracks over the North Atlantic and North Pacific oceans, highlighting the two main storm tracks. However, there are also marked differences between the 2 month types. While the North Atlantic storm track is more geographically confined in HMR months, the opposite is the case for the North Pacific storm track (Figure 5a compared to Figure 5b). Moreover, cyclones tracking over the Nordic seas, northeastern Europe, and western Russia are nearly absent in HMR months, with fewer cyclones ending up in the Arctic Ocean. Consequently, the AOCM is only weakly defined.

The contours in Figure 6 show the climatology of the storm track characteristics for the Northern Hemisphere summer. While most cyclones cross the North Pacific Ocean zonally and end around the Gulf of Alaska, storms track more northeastward over the North Atlantic Ocean (Figure 6a). Here cyclones continue either over the British Isles into southern Scandinavia, or north over Iceland, the Iceland-Greenland-Norwegian Seas and into the Arctic. Once the cyclones enter the Arctic, they are likely to die out in the region. Very few cyclones here originate over North America, largely explained by the strong

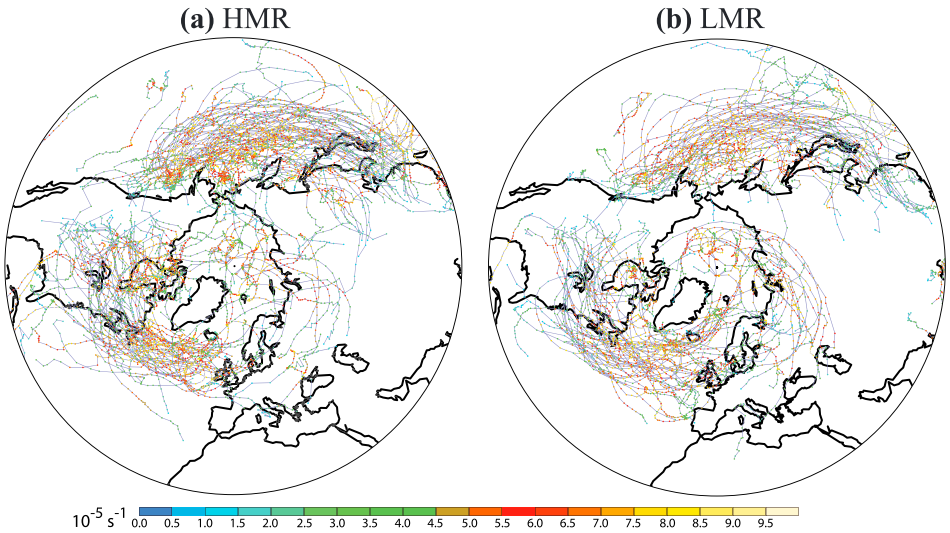

Figure 5. Cyclone tracks in composites of (a) HMR and (b) LMR months for MJJA 1979–2013. For visual clarity, only systems that last longer than 4 days travel farther than 1000 km and reach a maximum intensity over 8×10^{-5} s^{-1} are included. Blue lines denote tracks, while colored dots indicate the intensity at each 6-hourly time step along the track in units of 10^{-5} s^{-1}.

southward component of the jet stream flow, which tends to steer cyclones away from the Arctic Ocean [*Serreze and Barrett*, 2008].

The shading in Figure 6a corresponds to the difference in cyclone track tightness between Figures 5a and 5b. While more cyclones track into the Arctic from the Nordic seas and northern Russia in LMR months, significantly fewer track across these regions in HMR months. There is no clearly defined AOCM. In isolation, fewer cyclones results in higher pressure, but the prevalent anticyclonic tendencies in Figures 3a and 3b might also be precursors for the missing cyclones in the Arctic. The higher Arctic pressure contributes to zonal shifts of the North Atlantic and North Pacific jet streams (Figure 3c), with a tendency to block incoming Arctic cyclones and veer them on a more zonal path (Figure 6a).

In the North Pacific Ocean, the zonal shift of the storm track results in cyclones in HMR months track to the south of those in LMR months (Figure 6a). Additionally, 22% more cyclones track in the Sea of Japan (here defined 35°N–45°N, 130°E–140°E) in HMR compared to LMR months. Another maximum occurs over the British Isles (31% increase; here defined 50.5°N–58.5°N, 10°W–1°E), as the northeastward branch of the North Atlantic storm track is absent in HMR months. The result is 9% more cyclones tracking across Eurasia in a band about 50°N–60°N in HMR compared to LMR months. This coincides with the 8% u_{300} acceleration over this region (Figure 3c).

The mean intensity pattern (contours in Figure 6b) generally follows track density, with maxima over the North Pacific and North Atlantic oceans and, to a lesser extent, the Arctic Ocean. In other words, cyclones tracking in storm dense regions are generally stronger than the few cyclones tracking in climatologically more calm regions.

Cyclones are climatologically stronger over ocean than over land. In addition to a dependence on cyclone count distribution, changes in intensity with increased Arctic sea ice melt also vary with temperature patterns (shading in Figure 6b). A warmer land surface enhances the baroclinicity, increasing the potential of cyclone development.

Of the cyclones found over the Arctic Ocean, most stem from the North Atlantic Ocean or the Eurasian continent, if not having developed in the region. Cyclogenesis is closely related to topography, with large cyclone development around the Rocky Mountains, the European Alps, east Greenland coast, and the mountain regions around the Lake of Baikal (contours in Figure 6c). Around the Arctic Ocean, the topography over northeastern Siberia and northern Alaska helps to "trap" the cold Arctic air, sharpening the coastal baroclinicity and enhancing the cyclogenesis [*Serreze and Barry*, 2009b, and references therein].

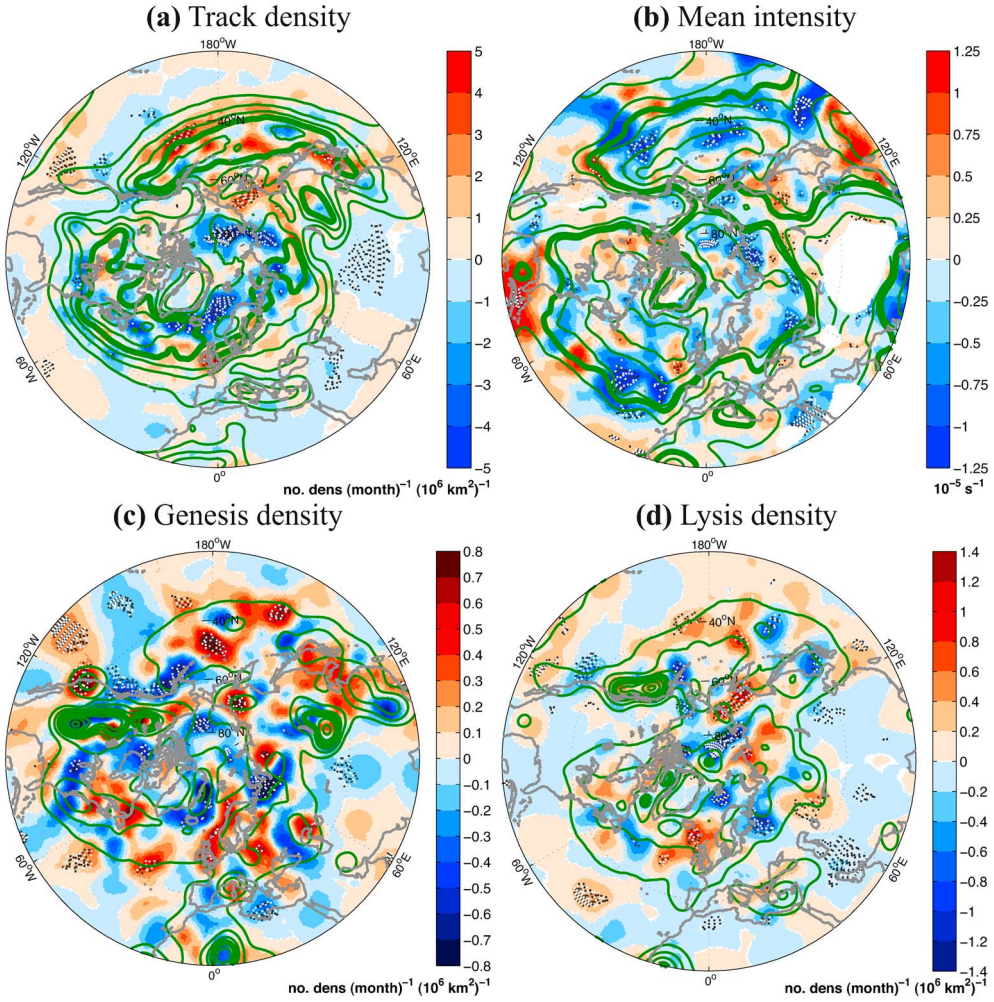

Figure 6. (a) Track density, (b) mean intensity, (c) gensis density, and (d) lysis density composites for HMR minus LMR months for MJJA 1979–2013. Green contours mark climatology over 1979–2013. Contour intervals are (Figure 6a) 2.5 number density (month)$^{-1}$(10^6 km^2)$^{-1}$, (Figure 6b) 0.75 × 10^{-5} s^{-1}, (Figures 6c and 6d) 0.5 number density (month)$^{-1}$(10^6 km^2)$^{-1}$, with bold contours for visual clarity representing (Figure 6a) 10 number density (month)$^{-1}$ (10^6 km^2)$^{-1}$, (Figures 6b) 3 × 10^{-5} s^{-1}, and (Figures 6c and 6d) 2 number density (month)$^{-1}$(10^6 km^2)$^{-1}$, respectively. Alternating black and white dots mark regions where $p < 0.05$. Regions with fewer than 0.5 number density (month)$^{-1}$(10^6 km^2)$^{-1}$ climatologically are shaded white in Figure 6b.

Except for these two regions, there is a marked drop in number of cyclones generated and dying out in the Arctic in HMR compared to LMR months (shading in Figures 6c and 6d). Over the Arctic Ocean (here defined circumpolar 75°N–90°N), cyclogenesis reduces by 17% and cyclolysis reduces by 16% in HMR months relative to climatology. Corresponding increases for LMR months are 8 and 5%, respectively.

The storm track characteristic changes in HMR compared to LMR months over the British Isles are especially interesting. While increases in track and lysis density (Figures 6a and 6d) follow from the reduced MSLP (Figure 3a) and Z_{300} (Figure 3b) and corresponding southward jet stream shift (Figure 3c), there is a small, insignificant decrease in mean intensity (Figure 6b). In other words, more cyclones reach the region in HMR months, but these are on average weaker than normal.

More cyclones are also developing over the British Isles (Figure 6c). Cyclogenesis can often take place northward of the jet streaks. In HMR months, the British Isles constitute the northward flank of the jet stream (Figure 3c). Additionally, enhanced secondary cyclogenesis, possibly along trailing cold fronts, might explain why there are more cyclones forming in HMR months here.

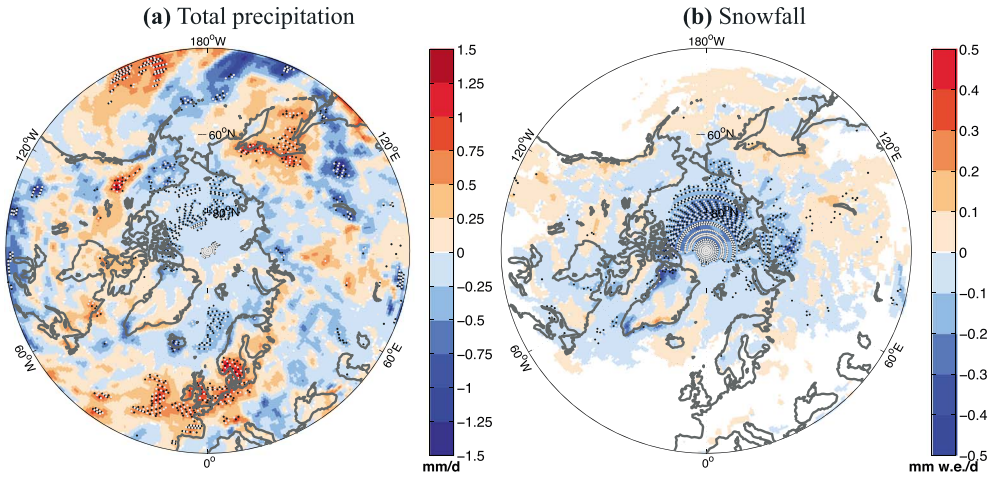

Figure 7. (a) Total precipitation and (b) snowfall composites for HMR minus LMR months for MJJA 1979–2013. Unit in Figure 7b is millimeter water equivalent per day (mm w.e./d). Alternating black and white dots mark regions of significant difference at a 95% confidence level. Note that latitude range is 40°N–90°N.

3.3. Precipitation and Snowfall

As expected from the anticyclonic tendency (Figures 3a and 3b) and missing AOCM (Figure 6a) in HMR relative to LMR months, on average 0.1 mm/d less precipitation falls over the Arctic Ocean (corresponding to 15% of the climatological mean; Figure 7a). Moreover, the increased pressure field causes a relatively strong northeasterly wind over the Norwegian Sea (Figure 3), which limits the cyclone frequency (Figure 6a) and significantly reduces the precipitation here (Figure 7a). In midlatitudes, on average 0.4 mm/d (equivalent to 21% of the climatological mean) more rain falls in northwestern Europe in HMR compared to LMR months (Figure 7a). This coincides with the increased cyclonic tendency (Figures 3a and 3b), the equatorward shift of the jet stream (Figure 3c), more southerly wind flow (Figure 3d) and increased cyclone activity (Figures 6a, 6c, and 6d).

The region around the Sea of Okhotsk (here defined 47.5°N–63.0°N, 135.0°E–165.0°E) is also significantly wetter in HMR compared to LMR months (Figure 7a), with an average difference of 0.4 mm/d (20% of the climatological mean). As in the northwestern Europe, this follows from the cyclonic tendency in the western branch of the region (Figures 3a and 3b), causing anomalous southerly wind flow (Figure 3d) and more cyclones tracking into (Figure 6a) and dying out (Figure 6d) in the region. However, the near-surface relative southerly wind is stronger in the Sea of Okhotsk, bringing warm and moist air from the North Pacific Ocean (Figure 3a). Moreover, the more zonally flowing jet stream over the North Pacific and North Atlantic oceans shifts "into" the Sea of Okhotsk while "out" of northwestern Europe (Figure 3c).

Snowfall in MJJA is confined to high latitudes. Higher snowfall implies lower pressure and more clouds. In summer, this reduces the incoming SW radiation and dampens the sea ice melt. Additionally, snowfall will increase the albedo of the ice, also reducing the melt. This explains the significantly reduced (enhanced) snowfall in HMR (LMR) months seen in Figure 7b. Over the Arctic Ocean, there is 0.1 mm w.e./d (equivalent to 39%) less snowfall in HMR compared to LMR months; that is, the reduction in snowfall constitutes the overall decrease in total precipitation. The circulation changes in HMR months (sections 3.1 and 3.2) eliminate the negative feedback the snowfall provides for sea ice through cloudiness and albedo as outlined above.

During August, the snow and ice melt rates reach their peak, leaving the sea ice albedo at its minimum [*Riihelä et al.*, 2013]. This makes the phase of precipitation over the Arctic even more important than in the other 3 months [*Riihelä et al.*, 2013]. Moreover, of the 4 months in Figure 7b, August sees the largest change in snowfall between HMR and LMR months (not shown). Nevertheless, the insolation in August is weaker than in the other MJJA months, limiting the albedo impact on the surface energy balance [*Curry et al.*, 1996].

3.4. Incoming Surface Radiation

The monthly mean Arctic cloud cover increases from May to August [*Curry et al.*, 1996]. Incoming SW radiation at the top of the atmosphere (TOA) reaches maximum in June in the Arctic. Hence, incoming SW

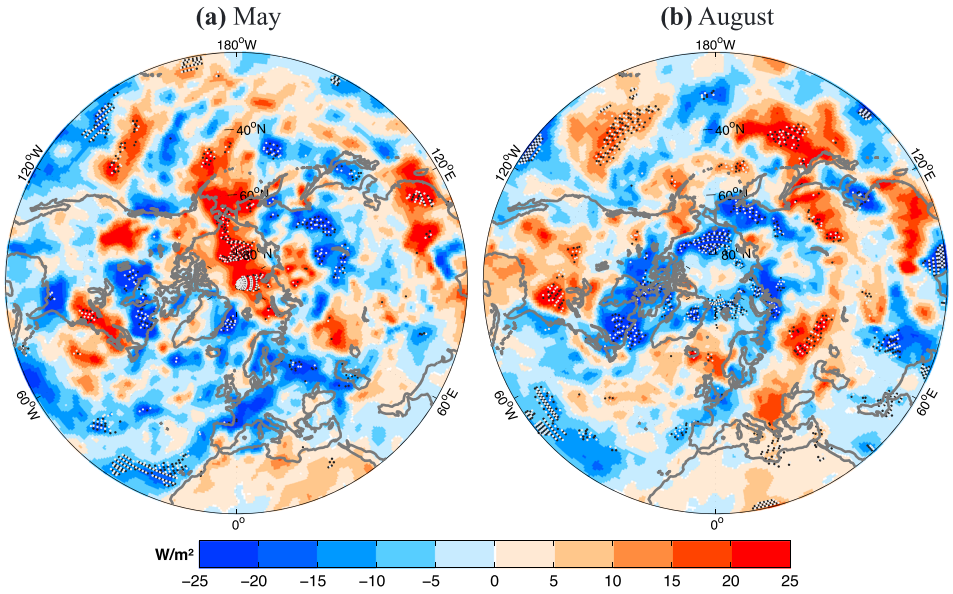

Figure 8. Incoming surface shortwave radiation composites for HMR minus LMR months for (a) May and (b) August 1979–2013. Positive direction is downward. Alternating black and white dots mark regions of significant difference at a 95% confidence level.

radiation at the surface (a function of SW radiation at TOA and cloud cover) has a maximum in June, with lower values in July and August than May.

From late fall to early spring, the Arctic surface radiation balance is dominated by LW radiation [*Curry et al.*, 1996]. However, due to the significant absorption of LW radiation in the atmosphere and reemission toward the surface, the net radiation balance is only weakly negative. In other words, the net surface cloud forcing is positive (warming the surface) throughout most of the year. The exception is mid-May to the end of June. Then the cloud-cooling effect of reflected incoming SW radiation surpasses the warming due to reemission of outgoing LW radiation [*Curry et al.*, 1996, and references therein].

Figures 8 and 9 present the difference between HMR and LMR months of incoming SW and LW radiation, respectively, at the surface. Here averages over May (five HMR and four LMR months) and August (five each of HMR and LMR months) months are presented rather than the MJJA season average to show the transition over the season. Positive direction is downward.

May HMR months are associated with reduced cloud cover over the Arctic, with the largest deviations from the central Arctic Ocean to the Bering Sea. This follows from the anomalous high incoming SW radiation (+9 W/m^2 over the Arctic Ocean; Figure 8a) and low incoming LW radiation (insignificant −1 W/m^2 over the Arctic Ocean; Figure 9a). The anticyclonic tendency here (Figure 3a) results in fewer clouds, which increases the SW radiation reaching the surface and enhances the sea ice melt.

In contrast, for August, less SW radiation (−7 W/m^2 over the Arctic Ocean; Figure 8b) and more LW radiation (+9 W/m^2 over the Arctic Ocean; Figure 9b) reach the surface in the marginal ice zone. The feature reveals a possible cloud feedback resulting from the diminishing sea ice: as the ocean surface evaporation increases with the retreating sea ice edge, clouds form near the sea ice boundaries [*Francis et al.*, 2009, and references therein]. The highest cloud formation takes place in the Barents, Kara, Beaufort, and East Siberian seas, coinciding with regions of largest SIC variance (reaching 26% lower SIC in HMR compared to LMR months; not shown). More LW radiation is absorbed and reemitted in the atmosphere, leading to a significant increase in incoming LW radiation at the surface in August HMR months (Figure 9b).

For the Greenland Sea (here defined 70°N–80°N, 0–20°W), incoming SW and LW radiation anomalies in May (Figures 8a and 9a) are comparable to those of the Arctic Ocean in August (Figures 8b and 9b). In May, anomalous low SIC (partly seen in Figure 2a) enhances cloud formation already this month, with changes of −23 and +15 W/m^2 for incoming SW and LW radiation, respectively.

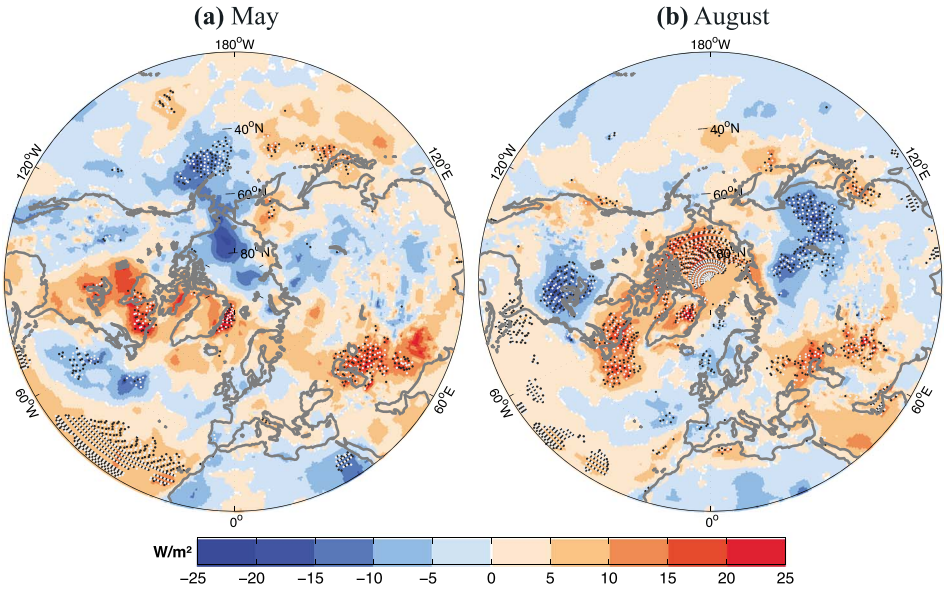

Figure 9. Incoming surface longwave radiation composites fo HMR minus LMR months for (a) May and (b) August 1979–2013. Positive direction is downward. Alternating black and white dots mark regions of significant difference at a 95% confidence level.

3.5. Surface Temperature

Altered atmospheric circulation can lead to altered T_s through heat advection. In summer, several effects will often give higher temperatures at the surface locally: enhanced incoming SW radiation associated with cloud suppressing higher pressure, lower heat loss due to reduced winds, and reduced latent heat loss from evaporation of water due to soil dryness.

Exploring these possibilities, the Arctic anticyclonic tendency (Figure 3a) is accompanied by generally higher temperatures (although with little significance; Figure 10) and enhanced sea ice melt (expressed by the composite HMR minus LMR months). Climatologically, snowfall makes up about one third of the total precipitation over the Arctic Ocean in MJJA. Due to the overall warming and thus heat advection into the region, this fraction is reduced to about one fourth in HMR months (not shown).

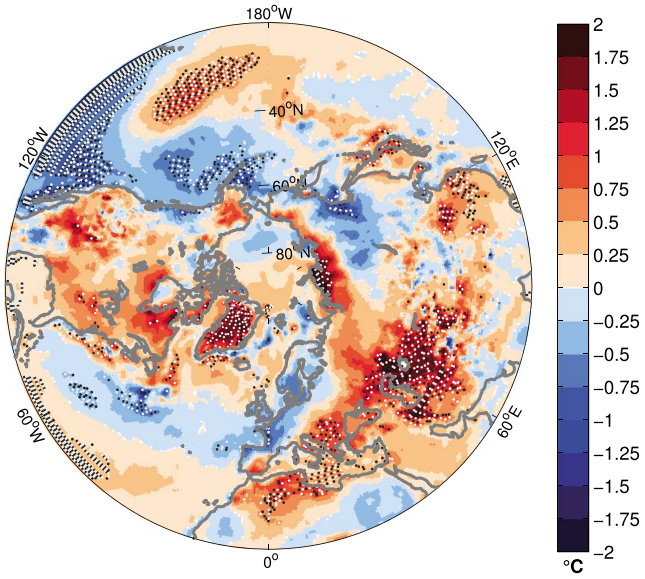

Figure 10. Surface temperature composites for HMR minus LMR months for MJJA 1979–2013. Alternating black and white dots mark regions of significant difference at a 95% confidence level.

The temperature signal over the Arctic Ocean in HMR months is nevertheless small compared to the warming along its coastal boundaries (average of 0.3°C compared to up to 2.0°C over the Taymyr Peninsula at 100°E). This is due to the fact that sea surface temperature will always be close to the freezing point in a partly ice covered ocean [*Rayner et al.*, 2003].

The coastal warming in HMR months strengthens the temperature gradient between the Arctic Ocean and the warmer continents in MJJA (Figure 10). Consequently, the baroclinicity strengthens and cyclogeneses increase in northeastern

Siberia and Alaska, which are regions of high cyclogenesis (Figure 6c). In the former region, the T_s and surface baroclinicity enhancements around the Taymyr peninsula (Figures 6c and 10) are opposite to the decrease in cyclone frequency (Figure 6a), resulting in a significant reduction in mean lifetime of the cyclones here (not shown).

Greenland is significantly warmer in HMR compared to LMR months, with differences generally in the range 1.0–2.7°C (Figure 10). This highlights the importance of the ice-albedo feedback in summertime: as the anticyclonic tendency enhances the southerly wind flow west of Greenland (Figures 3a and 3b), more heat and moisture are brought into the area, which amplify the snow melt and melt pond formation into the season [*McMillan et al.*, 2007; *Sundal et al.*, 2009]. This lowers the albedo, enhancing the melt potential per W/m^2 into the season. As for sea ice, the glacial ice melt promotes cloud development, pictured by reduced incoming SW (Figure 8b) and increased incoming LW radiation (Figure 9b). Moreover, the warming feature strengthens the hypothesized strong correlation between Arctic sea ice melt and Greenland ice sheet mass balance [*Rennermalm et al.*, 2009].

HMR months are associated with significant warming in a region from the Mediterranean Sea to central Asia, with T_s up to 2.4°C higher than LMR months (Figure 10). This is climatologically a dry region with few cyclones and little rainfall, which gets drier in HMR months (Figures 6a and 7a). Hence, the heat builds up through reduced cloud cover (seasonal mean similar to Figures 8b and 9b for the region). Moreover, in the dry and warm regions, drying of the soil might strengthen the initial warming in a positive soil moisture feedback [*Hirschi et al.*, 2011]. This follows from the anomalous high incoming LW radiation, especially in central Asia (Figure 9), which is a product of the enhanced outgoing LW radiation through the Stefan-Boltzmann law.

Eastern China, the Korean Peninsula, and Japan are also significantly warmer in HMR compared to LMR months (Figure 10). This is linked to an anomalous southerly airflow rather than local cloud cover and precipitation changes, with air advected from the climatologically warmer Pacific Ocean (Figure 3a).

One possible effect of the nearly coherent surface heating from the Mediterranean Sea to East Asia (Figure 10) is the development of thermal lows, in which the near-surface air warms and rises, as indicated by the reduced MSLP (Figure 3a). Aloft, this vertical airflow raises the 300 hPa pressure level, corresponding to the increase in Z_{300} over regions of enhanced T_s (Figures 3b and 10). The relative upper level ridges over eastern Mediterranean Sea, east of the Caspian Sea, and over Japan (Figure 3b) cause anomalous poleward airflows over central Europe, western Russia, and around the Sea of Okhotsk (Figure 3d). We may speculate that this warm air advection cools as it flows to high latitudes, where it sinks and contributes to the anticyclonic tendency seen in Figure 3a.

The Sea of Okhotsk, northwestern Europe, and the regions outside the Gulf of Alaska and off the coast of the Baja California peninsula all have lowered pressure (Figure 3a; insignificant for the two latter regions), enhanced cyclone activity (Figure 6a), and enhanced precipitation (Figure 7a; not shown for the latter region). This is associated with increases in cloud cover and latent heat absorption from evaporation of raindrops at the surface in HMR months (not shown). Both effects lower the temperature (Figure 10). Hence, summer months of anomalously high Arctic sea ice melt are both wetter and cooler than normal in these regions.

The anticorrelation between cyclone frequency and temperature is also pronounced over the midlatitude oceans. Areas of lowered (raised) T_s (Figure 10) generally coincide with areas of enhanced (reduced) synoptic activity (Figure 6a) and precipitation (Figure 7a).

4. Discussion

Our findings in Figure 3a support *Screen et al.* [2011] and *Ogi et al.* [2010] who linked summers of anomalous low sea ice to anticyclonic anomalies over the Arctic. However, the time period, season, data set, and methods are different in this study. Both *Screen et al.* [2011] and *Ogi et al.* [2010] based their analysis on September sea ice, with the former study a composite analysis on interannual variability and the latter a regression and trend analysis. Common for the two studies are the use of several summer months to explain the trailing anomalous September SIE. Here we rather isolated *all* summer months of anomalous sea ice *melt* and highlighted the *simultaneous* atmospheric patterns.

Furthermore, May through July (MJJ) summers preceding low September SIEs were characterized by reduced cloud cover over the Arctic Ocean in *Screen et al.* [2011]. On the basis of our analysis, we hypothesize that this is due to the strong signal in May, represented by the anomalous high incoming SW over the Arctic in Figure 8a. Only small changes occur in June and July (not shown), while the anomalous low SW in August (Figure 8b) argues for the positive cloud feedback mechanism near the sea ice margins suggested in section 3.4. This result follows *Liu et al.* [2012], who found a 0.36–0.47% increase in cloud cover for a 1% decrease in SIC from July to November 2000–2010. The largest cloud response, similar to Figure 8b, occurred in the Barents, Kara, Beaufort, and Chukchi Seas.

The anticyclonic tendency at sea level and at 300 hPa in the Arctic following from our composite analysis in Figures 3a and 3b also bear resemblance to the *Z* fields at 900, 500, and 200 hPa in *Tang et al.* [2013], resulting from a regression on detrended summer SIE index. Moreover, from self-organizing map pattern 3, *Feldstein and Lee* [2014] found an anomalous warming in the Barents and Kara seas associated with sea ice loss to enhance the climatological high, create stronger vertical wave activity flux into the stratosphere, and thus weaken the polar vortex. Although for winter (December, January, and February), their results bear resemblance to the MJJA MSLP and u_{300} patterns for HMR months in our Figures 3a, 3c, and 4.

With enhanced baroclinicity in the coastal Arctic regions in HMR compared to LMR months (Figure 10), one might expect a stronger subpolar jet stream and eddy activity in the region. However, we find that the jet and the AOCM are significantly weakened (Figures 3c, 4, and 6a). Similar to *Nishii et al.* [2014], we thus find that intraseasonal variations in the AOCM are not governed by this meridional T_s gradient. Instead, it appears as if the anticyclonic tendency discussed in section 3.1 is the governing factor.

Screen [2013] isolated the 10% wettest and driest summers over northern Europe, ending up with an anomalous wind field at 300 hPa similar to the results presented here (Figures 3c and 3d). This highlights the close linkage between anomalous Arctic sea ice and precipitation in northern Europe.

Moreover, *Screen* [2013] indicated the influence of unusual low Arctic sea ice on north European rainfall by compositing low and high ice model runs. These runs were based on SIC from one single year each. Nevertheless, the resulting precipitation pattern suggested wetter (drier) summers in northern (southern) Europe, as indicated by Figure 7a presented here. *Screen* [2013] linked the precipitation pattern to a southward displacement of the polar jet stream off the west coast of Europe. In Figures 3b and 3c, we show that not only is the jet stream shifted equatorward over the North Atlantic Ocean in HMR months but also strengthened as it reaches land over western and southwestern Europe. This coincides with a northward veering over central Europe (Figures 3b and 3d), advecting more moist subtropical air in the warm sectors of the cyclones associated with the warm conveyor belt flow [*Browning and Roberts*, 1994], consequently leading to more rainfall.

With a more zonal jet stream, more cyclones track across the North Atlantic Ocean into northern Europe instead of the Arctic (Figure 6a). *Screen et al.* [2011] discovered that fewer cyclones tracking into the Arctic in MJJ favored lower September SIE. Using an empirical orthogonal function analysis, *Dong et al.* [2013] found a significant anticorrelation between cyclones entering the Arctic and those reaching northwestern Europe of −0.61. They linked the two distinct North Atlantic paths to the summer NAO and blocking frequency over the United Kingdom and northwestern Europe. Here we find that only 5% of the anomalous sea ice melt underlying the cyclonic tendency can be explained by the NAO. In fact, not more than 10% of our sea ice melt index is due to any of the climate patterns analyzed (NAO, AO, and BSH). Our Figures 3a, 3b, 3d, and 10 bear some resemblance to the results dominated by the Arctic Dipole in *Overland et al.* [2012]. This is expected since half of their data (June 2007–2012) are included in our HMR months. However, for the rest of our time period (1979–2013), we find low coincidence between their Figure 2 and our LMR and HMR months in Figure 1. Finally, although there are some similarities to the features in Figures 3b, 3c, and 4 here, we do not find the negative summer Northern Annular Mode (NAM) in *Tachibana et al.* [2010] to demonstrate the observed atmospheric patterns in our study.

Dong et al. [2013] further isolated the wetter summers in England and Wales to more rainy days rather than changes in rain intensity or very heavy rainy days. This feature follows from Figure 3a, where cloudier days (not shown) generally increase the chance of rainfall. Moreover, the latent heat uptake (not shown) and reduced SW radiation (Figure 8) that follows, cool the air (Figure 10), with lower capacity for holding moisture.

Our hypothesized cloud feedback in section 3.4 offers an alternative explanation to *Kapsch et al.* [2013]. They suggested that anomalous low Arctic sea ice in September could be characterized by increasing LW radiation (and hence greenhouse effect) in spring and increasing absorption of SW radiation into the season as the ice melts. Our results show that the anticyclonic tendency (Figures 3a and 3b) reduces the cloud cover at the end of spring and enhances the incoming SW radiation (Figure 8a). As the sea ice melt accelerates, clouds form in the marginal ice zone (Figure 8b) and increase the greenhouse effect through positive LW radiation anomalies (Figure 9b). A positive cloud feedback emerges.

The T_s signal in Figure 10 has noticeable similarities with the pattern of surface air temperature resulting from reduced SIE/snow cover extent indices in *Tang et al.* [2013]. Over land, they linked this pattern to probability of extreme heat events, indicating that the significant warming in our Figure 10 might have severe consequences locally.

Figure 10 is also indicating a northward displacement of the Gulf Stream. This shift was also found by *Sato et al.* [2014], with an associated warming anomaly and thus sea ice loss in the Barents Sea. However, since they analyzed December 1979–2010, our apparent anticorrelation between MJJA T_s (Figure 10) and cyclone frequency (Figure 6a) and thus precipitation (Figure 7a) (cf. section 3.5) is not demonstrated in *Sato et al.* [2014].

5. Summary and Conclusion

The analyses performed in this study indicate distinct features linking summer months of anomalous Arctic sea ice melt to anomalous atmospheric circulation, with consequences for precipitation, radiation, and temperature. By standardizing the sea ice melts over the 140 MJJA months from 1979 to 2013, we end up with composites of 23 high (HMR) and 17 low (LMR) melt months.

In the Arctic, HMR months coincide with an anticyclonic tendency (up to 7 hPa; Figure 3a), which enhances the incoming SW radiation at the start of the summer (average of 9 W/m^2 over the Arctic Ocean; Figure 8a) and warms the region in general (0.3°C over the Arctic Ocean, up to 2.7°C over Greenland; Figure 10). This atmospheric circulation is associated with a tendency of storms to veer away from the Arctic on a more zonal path (Figure 6a), leaving the Arctic drier (average reduction of 0.1 mm/d over the Arctic Ocean; Figure 7a) with lowered albedo (represented by the equally sized reduction in snowfall in Figure 7b). A positive snow-albedo feedback emerges.

In August, the enhanced ocean surface evaporation from the retreating sea ice promotes cloud development (represented by the 7 W/m^2 reduced incoming SW radiation in Figure 8b and 9 W/m^2 increased incoming LW radiation in Figure 9b). Coming into late summer, reemission of LW radiation surpasses incoming SW radiation at the surface [*Curry et al.*, 1996]. Hence, the clouds trap heat, providing a mechanism for a positive cloud feedback.

In midlatitudes, cyclones track more zonally across the North Atlantic and North Pacific oceans in HMR compared to LMR months (Figure 6a). Consequently, HMR months are characterized as cloudier (Figure 8), wetter (Figure 7a), and cooler (Figure 10) in most of northern Europe and around the Sea of Okhotsk.

Farther south are HMR months associated with significant heating in a band from the Mediterranean Sea to East Asia (up to 2.4°C; Figure 10). This is linked to a partly significant increase (decrease) in u_{300} north (south) of the region through the thermal wind relationship (Figure 3c). Moreover, the resulting rising air (Figure 3a) is transported poleward (Figures 3b and 3d), where it cools, sinks, and possibly contributes to the increase of the MSLP (Figure 3a).

A few limitations of the method used in this study should be pointed out. First, the nondetrended SIE time series causes an uneven distribution of summer months over the time period (Figure 1). The overweight of recent summers in the HMR months includes trends in other parameters. Most evident, the global warming signal in T_s makes it hard to isolate the effect of Arctic sea ice loss on, for example, heat extremes.

On the latter link, the theory first put forward by *Francis and Vavrus* [2012] has received a lot of attention. They linked the AA and sea ice loss to slower moving and larger amplitude upper level Rossby waves, with an increase in probability of midlatitude extreme weather as a result. However, their findings have been extensively discussed [*Cohen et al.*, 2014; *Walsh*, 2014] and criticized [*Barnes*, 2013]. Results in our study indicate a more zonally flowing subtropical jet stream and cyclone tracks over the North Atlantic and North

Pacific oceans in connection with a significant weakening of the subpolar jet stream in HMR compared to LMR months (Figures 3c and 4). However, we find no clear evidence of a slowdown of the jet streams outside the Arctic (Figures 3c and 4), with reduced rather than enhanced meandering, as indicated by the bluish (reddish) color over solid (dashed) lines in Figure 3d. These partly contradictory results to *Francis and Vavrus* [2012] might reside in the differences between the methods used (cf. section 2), indicating the sensitivity of the proposed link to methodology, as found by *Barnes* [2013].

Second, our results do not imply causalities. A remote influence from tropical low-frequency variability could be the cause of both the concomitant anomalies in extratropical circulation and sea ice that we diagnosed. For example, *Ding et al.* [2014] proposed a Rossby wave link from the eastern Pacific Ocean to the Arctic to explain the recent warm anomalies over the Arctic, Greenland, and northeastern Canada.

Third, our study relied on atmospheric reanalysis and sea ice data only. Hence, possible changes in oceanic heat content or oceanic heat transport affecting sea ice melt and atmospheric parameters from below are not included. Fourth, except for the sea ice parameters, all data are from the ERA-Interim reanalysis. Although considered to be among the best data sets for the sparsely observed Arctic [*Hodges et al.*, 2011; *Chung et al.*, 2013; *Zappa et al.*, 2013], it is not free of errors [*Jakobson et al.*, 2012]. Nevertheless, with a focus on qualitative changes between high and low sea ice melt months rather than absolute numbers, we argue that the use of ERA-Interim is suitable for this study.

Fifth, an obvious question is whether the atmosphere leads the Arctic sea ice or vice versa. Numerous studies have tried to isolate the effect of the atmospheric circulation on the sea ice [e.g., *Deser and Teng*, 2008b; *Ogi et al.*, 2010, and references therein], with a corresponding quantity of analyses from the sea ice on the atmosphere [e.g., *Vihma*, 2014, and references therein]. Although out of the scope for this study, section 3.4 indicates a cloud feedback, where the atmosphere not only forces the sea ice in the start of summer but also show local responses to the sea ice anomalies at the end of the season. We do not assess to what extent these local responses causes large-scale circulation changes and possibly rapid reduction in ice cover.

With climate models simulating a strengthening of the AA, understanding the reasons for and consequences of anomalous Arctic sea ice melt is of high interest, stretching beyond the scientific community. Targeted modeling studies will add robustness to the number of anomalous summer sea ice melt months, as well as leading to a more thorough analysis of the dynamical linkages involved.

Acknowledgments

The data for this paper are available at NSIDC's web page Sea Ice Concentrations from Nimbus-7 SMMR and DMSP SSM/I-SSMIS Passive Microwave Data (http://nsidc.org/data/docs/daac/nsidc0051_gsfc_seaice.gd.html), at ECMWF's ERA-Interim web access (http://apps.ecmwf.int/datasets/data/interim_full_moda/), and at NOAA's NAO (http://www.cpc.ncep.noaa.gov/data/teledoc/nao.shtml) and AO (http://www.cpc.ncep.noaa.gov/products/precip/CWlink/daily_ao_index/ao.shtml) web pages. The work was financially supported by the Research Council of Norway through the BlueArc project (207650) and ACPCA project (223046). We wish to thank the two anonymous reviewers who provided constructive suggestions that improved the manuscript.

References

Barnes, E. (2013), Revisiting the evidence linking Arctic amplification to extreme weather in midlatitudes, *Geophys. Res. Lett.*, *40*, 4734–4739, doi:10.1002/grl.50880.

Bekryaev, R., I. Polyakov, and V. Alexeev (2010), Role of polar amplification in long-term surface air temperature variations and modern Arctic warming, *J. Clim.*, *23*(14), 3888–3906, doi:10.1175/2010JCLI3297.1.

Bengtsson, L., K. I. Hodges, and E. Roeckner (2006), Storm tracks and climate change, *J. Clim.*, *19*(15), 3518–3543, doi:10.1175/JCLI3815.1.

Browning, K. A., and N. M. Roberts (1994), Structure of a frontal cyclone, *Q. J. R. Meteorol. Soc.*, *120*(520), 1535–1557, doi:10.1002/qj.49712052006.

Budikova, D. (2009), Role of Arctic sea ice in global atmospheric circulation: A review, *Global Planet. Change*, *68*(3), 149–163, doi:10.1016/j.gloplacha.2009.04.001.

Cavalieri, D. J., C. L. Parkinson, P. Gloersen, and H. Zwally (1996), Sea Ice Concentrations from Nimbus-7 SMMR and DMSP SSM/I-SSMIS Passive Microwave Data, subset 1979–2013, 40°N–90°N, http://nsidc.org/data/docs/daac/nsidc0051_gsfc_seaice.gd.html, NASA Natl. Snow and Ice Data Cent. Distributed Active Archive Center, Boulder, Colo.

Chung, C., H. Cha, T. Vihma, P. Räisänen, and D. Decremer (2013), On the possibilities to use atmospheric reanalyses to evaluate the warming structure in the Arctic, *Atmos. Chem. Phys.*, *13*(22), 11,209–11,219, doi:10.5194/acp-13-11209-2013.

Cohen, J., et al. (2014), Recent Arctic amplification and extreme mid-latitude weather, *Nat. Geosci.*, *7*(9), 627–637, doi:10.1038/ngeo2234.

Coumou, D., V. Petoukhov, S. Rahmstorf, S. Petri, and H. J. Schellnhuber (2014), Quasi-resonant circulation regimes and hemispheric synchronization of extreme weather in boreal summer, *Proc. Natl. Acad. Sci*, *111*(34), 12,331–12,336, doi:10.1073/pnas.1412797111.

Curry, J., J. Schramm, W. Rossow, and D. Randall (1996), Overview of Arctic cloud and radiation characteristics, *J. Clim.*, *9*(8), 1731–1764, doi:10.1175/1520-0442.

Dee, D., et al. (2011), The ERA-Interim reanalysis: Configuration and performance of the data assimilation system, *Q. J. R. Meteorol. Soc.*, *137*(656), 553–597, doi:10.1002/qj.828.

Deser, C., and H. Teng (2008a), Recent trends in Arctic sea ice and the evolving role of atmospheric circulation forcing, 1979–2007, in *Arctic Sea Ice Decline: Observations, Projections, Mechanisms, and Implications*, edited by E. T. DeWeaver, C. M. Bitz, and L.-B. Tremblay, AGU, Washington, D. C., doi:10.1029/180GM03.

Deser, C., and H. Teng (2008b), Evolution of Arctic sea ice concentration trends and the role of atmospheric circulation forcing, 1979–2007, *Geophys. Res. Lett.*, *35*, L02504, doi:10.1029/2007GL032023.

Ding, Q., J. M. Wallace, D. S. Battisti, E. J. Steig, A. J. Gallant, H.-J. Kim, and L. Geng (2014), Tropical forcing of the recent rapid Arctic warming in northeastern Canada and Greenland, *Nature*, *509*(7499), 209–212, doi:10.1038/nature13260.

Dong, B., R. Sutton, T. Woollings, and K. I. Hodges (2013), Variability of the North Atlantic summer storm track: Mechanisms and impacts on European climate, *Environ. Res. Lett.*, *8*(3), 034037, doi:10.1088/1748-9326/8/3/034037.

Enomoto, T., B. J. Hoskins, and Y. Matsuda (2003), The formation mechanism of the Bonin high in August, *Q. J. R. Meteorol. Soc.*, *129*(587), 157–178, doi:10.1256/qj.01.211.

Feldstein, S. B., and S. Lee (2014), Intraseasonal and interdecadal jet shifts in the Northern Hemisphere: The role of warm pool tropical convection and sea ice, *J. Clim.*, *27*(17), 6497–6518, doi:10.1175/JCLI-D-14-00057.1.

Francis, J. A., and S. Vavrus (2012), Evidence linking Arctic amplification to extreme weather in mid-latitudes, *Geophys. Res. Lett.*, *39*, L06801, doi:10.1029/2012GL051000.

Francis, J. A., D. White, J. Cassano, W. Gutowski, L. Hinzman, M. Holland, M. Steele, and C. Vörösmarty (2009), An arctic hydrologic system in transition: Feedbacks and impacts on terrestrial, marine, and human life, *J. Geophys. Res.*, *114*, G04019, doi:10.1029/2008JG000902.

Hirschi, M., S. I. Seneviratne, V. Alexandrov, F. Boberg, C. Boroneant, O. B. Christensen, H. Formayer, B. Orlowsky, and P. Stepanek (2011), Observational evidence for soil-moisture impact on hot extremes in southeastern Europe, *Nat. Geosci.*, *4*(1), 17–21, doi:10.1038/ngeo1032.

Hodges, K. I. (1994), A general method for tracking analysis and its application to meteorological data, *Mon. Weather Rev.*, *122*(11), 2573–2586, doi:10.1175/1520-0493(1994)122<2573:AGMFTA>2.0.CO;2.

Hodges, K. I. (1995), Feature tracking on the unit-sphere, *Mon. Weather Rev.*, *123* (12), 3458–3465, doi:10.1175/1520-0493(1995)123<3458:FTOTUS>2.0.CO;2.

Hodges, K. I. (1996), Spherical nonparametric estimators applied to the UGAMP model integration for AMIP, *Mon. Weather Rev.*, *124*, 2914–2932, doi:10.1175/1520-0493(1996)124<2914:SNEATT>2.0.CO;2.

Hodges, K. I. (1999), Adaptive constraints for feature tracking, *Mon. Weather Rev.*, *127* (6), 1362–1373, doi:10.1175/1520-0493(1999)127<1362:ACFFT>2.0.CO;2.

Hodges, K. I. (2008), Confidence intervals and significance tests for spherical data derived from feature tracking, *Mon. Weather Rev.*, *136*(5), 1758–1777, doi:10.1175/2007MWR2299.1.

Hodges, K. I., R. Lee, and L. Bengtsson (2011), A comparison of extratropical cyclones in recent reanalyses ERA-Interim, NASA MERRA, NCEP CFSR, and JRA-25, *J. Clim.*, *24*(18), 4888–4906, doi:10.1175/2011JCLI4097.1.

Jakobson, E., T. Vihma, T. Palo, L. Jakobson, H. Keernik, and J. Jaagus (2012), Validation of atmospheric reanalyses over the central Arctic Ocean, *Geophys. Res. Lett.*, *39*, L10802, doi:10.1029/2012GL051591.

Kapsch, M.-L., R. G. Graversen, and M. Tjernström (2013), Springtime atmospheric energy transport and the control of Arctic summer sea-ice extent, *Nat. Clim. Change*, *3*(8), 744–748, doi:10.1038/nclimate1884.

Liu, Y., J. Key, Z. Liu, X. Wang, and S. Vavrus (2012), A cloudier Arctic expected with diminishing sea ice, *Geophys. Res. Lett.*, *39*, L05705, doi:10.1029/2012GL051251.

McMillan, M., P. Nienow, A. Shepherd, T. Benham, and A. Sole (2007), Seasonal evolution of supra-glacial lakes on the Greenland Ice Sheet, *Earth Planet. Sci. Lett.*, *262*(3), 484–492, doi:10.1016/j.epsl.2007.08.002.

Mesquita, M., N. Kvamstø, A. Sorteberg, and D. Atkinson (2008), Climatological properties of summertime extra-tropical storm tracks in the Northern Hemisphere, *Tellus A*, *60*(3), 557–569, doi:10.1111/j.1600-0870.2008.00305.x.

Nansen, F. (1902), *The Oceanography of the North Polar Basin, Norwegian North Polar Expedition, 1893–1896: Scientific Results*, vol. 3, pp. 357–386, Longmans, Green & Co., Harlow, U. K.

Neyman, J., and E. Pearson (1933), On the problem of the most efficient tests of statistical hypotheses, *Philos. Trans. R. Soc. London, Ser. A*, *231*, 289–337, doi:10.1098/rsta.1933.0009.

Nishii, K., H. Nakamura, and Y. J. Orsolini (2014), Arctic summer storm track in CMIP3/5 climate models, *Clim. Dyn.*, *44*, 1–17, doi:10.1007/s00382-014-2229-y.

Ogi, M., K. Yamazaki, and J. Wallace (2010), Influence of winter and summer surface wind anomalies on summer Arctic sea ice extent, *Geophys. Res. Lett.*, *37*, L07701, doi:10.1029/2009GL042356.

Orsolini, Y. J., and A. Sorteberg (2009), Projected changes in Eurasian and Arctic summer cyclones under global warming in the Bergen Climate Model, *Atmos. Oceanic Sci. Lett.*, *2*(1), 62–67.

Overland, J. E., J. A. Francis, E. Hanna, and M. Wang (2012), The recent shift in early summer Arctic atmospheric circulation, *Geophys. Res. Lett.*, *39*, L19804, doi:10.1029/2012GL053268.

Rayner, N., D. Parker, E. Horton, C. Folland, L. Alexander, D. Rowell, E. Kent, and A. Kaplan (2003), Global analyses of sea surface temperature, sea ice, and night marine air temperature since the late nineteenth century, *J. Geophys. Res.*, *108*(D14), 4407, doi:10.1029/2002JD002670.

Rennermalm, A., L. Smith, J. Stroeve, and V. Chu (2009), Does sea ice influence Greenland ice sheet surface-melt?, *Environ. Res. Lett.*, *4*(2), 024011, doi:10.1088/1748-9326/4/2/024011.

Riihelä, A., T. Manninen, and V. Laine (2013), Observed changes in the albedo of the Arctic sea-ice zone for the period 1982–2009, *Nat. Clim. Change*, *3*(10), 895–898, doi:10.1038/nclimate1963.

Sato, K., J. Inoue, and M. Watanabe (2014), Influence of the Gulf Stream on the Barents Sea ice retreat and Eurasian coldness during early winter, *Environ. Res. Lett.*, *9*(8), 084009, doi:10.1088/1748-9326/9/8/084009.

Screen, J. A. (2013), Influence of Arctic sea ice on European summer precipitation, *Environ. Res. Lett.*, *8*(4), 044015, doi:10.1088/1748-9326/8/4/044015.

Screen, J. A., and I. Simmonds (2010), The central role of diminishing sea ice in recent Arctic temperature amplification, *Nature*, *464*(7293), 1334–1337, doi:10.1038/nature09051.

Screen, J. A., and I. Simmonds (2013), Exploring links between Arctic amplification and mid-latitude weather, *Geophys. Res. Lett.*, *40*, 959–964, doi:10.1002/GRL.50174.

Screen, J. A., I. Simmonds, and K. Keay (2011), Dramatic interannual changes of perennial Arctic sea ice linked to abnormal summer storm activity, *J. Geophys. Res.*, *116*, D15105, doi:10.1029/2011JD015847.

Screen, J. A., C. Deser, I. Simmonds, and R. Tomas (2013), Atmospheric impacts of Arctic sea-ice loss, 1979–2009: Separating forced change from atmospheric internal variability, *Clim. Dyn.*, *43*, 333–344, doi:10.1007/s00382-013-1830-9.

Serreze, M., and J. Francis (2006), The Arctic amplification debate, *Clim. Change*, *76*(3-4), 241–264, doi:10.1007/s10584-005-9017-y.

Serreze, M., and A. Barrett (2008), The summer cyclone maximum over the Central Arctic Ocean, *J. Clim.*, *21*(5), 1048–1065, doi:10.1175/2007JCLI1810.1.

Serreze, M., and R. Barry (2009a), Arctic Ocean–sea ice–climate interactions, in *The Arctic Climate System*, pp. 177–207, Cambridge Univ. Press, Cambridge, U. K.

Serreze, M., and R. Barry (2009b), The atmospheric circulation, in *The Arctic Climate System*, pp. 74–109, Cambridge Univ. Press, Cambridge, U. K.

Smedsrud, L., A. Sirevaag, K. Kloster, A. Sorteberg, and S. Sandven (2011), Recent wind driven high sea ice area export in the Fram Strait contributes to Arctic sea ice decline, *The Cryosphere*, *5*(4), 821–829, doi:10.5194/tc-5-821-2011.

Sorteberg, A., and B. Kvingedal (2006), Atmospheric forcing on the Barents Sea winter ice extent, *J. Clim.*, *19*(19), 4772–4784, doi:10.1175/JCLI3885.1.

Sorteberg, A., and J. E. Walsh (2008), Seasonal cyclone variability at 70°N and its impact on moisture transport into the Arctic, *Tellus A*, *60*(3), 570–586, doi:10.1111/j.1600-0870.2008.00314.x.

Stroeve, J., V. Kattsov, A. Barrett, M. Serreze, T. Pavlova, M. Holland, and W. Meier (2012), Trends in Arctic sea ice extent from CMIP5, CMIP3 and observations, *Geophys. Res. Lett.*, *39*, L16502, doi:10.1029/2012GL052676.

Stroeve, J., T. Markus, L. Boisvert, J. Miller, and A. Barrett (2014), Changes in Arctic melt season and implications for sea ice loss, *Geophys. Res. Lett.*, *41*, 1216–1225, doi:10.1002/2013GL058951.

Sundal, A. V., A. Shepherd, P. Nienow, E. Hanna, S. Palmer, and P. Huybrechts (2009), Evolution of supra-glacial lakes across the Greenland Ice Sheet, *Remote Sens. Environ.*, *113*(10), 2164–2171, doi:10.1016/j.rse.2009.05.018.

Tachibana, Y., T. Nakamura, H. Komiya, and M. Takahashi (2010), Abrupt evolution of the summer Northern Hemisphere annular mode and its association with blocking, *J. Geophys. Res.*, *115*, D12125, doi:10.1029/2009JD012894.

Tang, Q., X. Zhang, and J. A. Francis (2013), Extreme summer weather in northern mid-latitudes linked to a vanishing cryosphere, *Nat. Clim. Change*, *4*(1), 45–50, doi:10.1038/nclimate2065.

Thorndike, A., and R. Colony (1982), Sea ice motion in response to geostrophic winds, *J. Geophys. Res.*, *87*(C8), 5845–5852, doi:10.1029/JC087iC08p05845.

Vihma, T. (2014), Effects of Arctic sea ice decline on weather and climate: A review, *Surv. Geophys.*, *35*, 1175–1214, doi:10.1007/s10712-014-9284-0.

Walsh, J. E. (2014), Intensified warming of the Arctic: Causes and impacts on middle latitudes, *Global Planet. Change*, *117*, 52–63, doi:10.1016/j.gloplacha.2014.03.003.

Wang, M., and J. E. Overland (2012), A sea ice free summer Arctic within 30 years: An update from CMIP5 models, *Geophys. Res. Lett.*, *39*, L18501, doi:10.1029/2012GL052868.

Wernli, H., and C. Schwierz (2006), Surface cyclones in the ERA-40 dataset (1958–2001). Part I: Novel identification method and global climatology, *J. Atmos. Sci.*, *63*(10), 2486–2507, doi:10.1175/JAS3766.1.

Zappa, G., L. Shaffrey, and K. I. Hodges (2013), The ability of CMIP5 models to simulate North Atlantic extratropical cyclones, *J. Clim.*, *26*(15), 5379–5396, doi:10.1175/JCLI-D-12-00501.1.

Zhang, X., J. E. Walsh, J. Zhang, U. Bhatt, and M. Ikeda (2004), Climatology and interannual variability of Arctic cyclone activity: 1948–2002, *J. Clim.*, *17*(12), 2300–2317, doi:10.1175/1520-0442(2004)017<2300:CAIVOA>2.0.CO;2.